Supporting information

Janus Porous Membrane with Conical Nano-needle Channel for Rapid Unidirectional Water Transport

Zhecun Wang,[a,c] Yonggang Li,[a] Shenghai Li,*[a,b] Jing Guo* [a,b] and Suobo Zhang[a,b]

[a]Key Laboratory of Polymer Ecomaterials, Changchun Institute of Applied Chemistry, Chinese Academy of Sciences, Changchun 130022, P. R. China.
[b]University of Science and Technology of China, Hefei 230026, P. R. China
[c]University of Chinese Academy of Sciences, Beijing 100049, P. R. China.
*Corresponding author lsh@ciac.ac.cn Fax: 86-431-85685653; Tel: 86-431-85262117

Video S1 the water (10 μL) is unidirectional transported from the hydrophobic face to the hydrophilic face (PNJPM-20)
Video S2 the water (10 μL) is blocked from the hydrophilic face to the hydrophobic face (PNJPM-20)

Materials and experiments

Materials

Copper mesh (mesh number: 16) and steel needles (length: 4.4 cm) were purchased from the market. The poly (vinylidene fluoride-co-hexafluoro propylene) (PVDF-HFP, M_w = 400 000 g mol^{-1}), dodecyl mercaptan, sodium hydroxide, Reactive Red 120, and ammonium persulfate were purchased from Sigma. All other solvents were in chemically pure grade and used as purchased unless otherwise noted.

Electrospinning method to fabricate the hydrophobic membrane

The PVDF-HFP solution was prepared by dissolving PVDF-HFP (16 g) in 100 mL solvent mixture of DMF and acetone (50:50 vol/vol). The homogeneous hydrophobic membranes (PVDF-HFP) were prepared by electrospinning the respective solutions using a needle electrospinning setup (20 KV, rate: 0.5 mL/h, receiving distance on tinfoil: 15 cm). The thickness of the membrane was controlled by electrospinning time (20 s, 40 s, 60 s). We measured the thickness of 30 min by a thickness gage, and the thickness of different time (20 s, 40 s, 60 s) was calculated by the thickness of 30 min. The morphology and pore size were obtained by scanning electron microscope (SEM, Philips XL30 ESEM FEG).

Fabrication of the JPMs

All the copper meshes were immersed in 1 M HCl solution to remove surface impurities, followed by rinsing three times with deionized water.

The JPMs and PNJPMs: The precleaned copper meshes were etched in aqueous solution of 2.5 M NaOH and 0.15 M $(NH_4)_2S_2O_8$ for 20 min at room temperature. After etching reaction, the resultant meshes were washed with deionized water. The dried solution oxidized copper mesh was attached to the tinfoil, and the PVDF-HFP solution was electrospun to the copper mesh for different time (20 s, 40 s, 60 s) forming the JPMs. The JPMs were blown by the N_2 vertically to gain the same pore size with the copper mesh to form the PNJPMs.

The heat oxidized Janus copper mesh: The precleaned copper meshes were oxidized at 500ºC for 30 min. The heat oxidized copper mesh was attached to the tinfoil, and the PVDF-HFP solution was electrospun to the copper mesh for different time (10 s and 20 s). After that, the JPM (electrospinning time of 20 s) was blown by N_2 vertically to gain the same pore size with the copper mesh.

Water motion on steel conical needle

All the steel needles were washed by the ethanol and deionized water to remove surface impurities. The washed steel needles were oxidized at 500ºC for 30 min to form the hydrophilic needles. The water (5 μL, dyed by Reactive Red 120) was dropped to the needles' tip (original hydrophobic needle and hydrophilic needle). The water's movement was recorded by a Canon digital SLR camera.

Characterization

The water contact angles were obtained by Drop Shape Analysis DSA10 (Krüss Gmbh, Germany) at ambient temperature with a droplet of 5 μL in volume. The videos on water penetration (unidirectional water transport) were recorded using Canon IXUS 115 HS digital camera and the Drop Shape Analysis DSA10 (Krüss Gmbh, Germany) at room temperature. The morphology was obtained by scanning electron microscope (SEM, Philips XL30 ESEM FEG).

Results and discussion

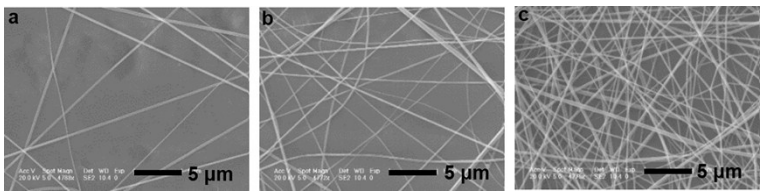

Fig. S1 The morphology of the PVDF-HFP membranes with different electrospinning time: (a) 20 s, (b) 40 s, (c) 60 s.

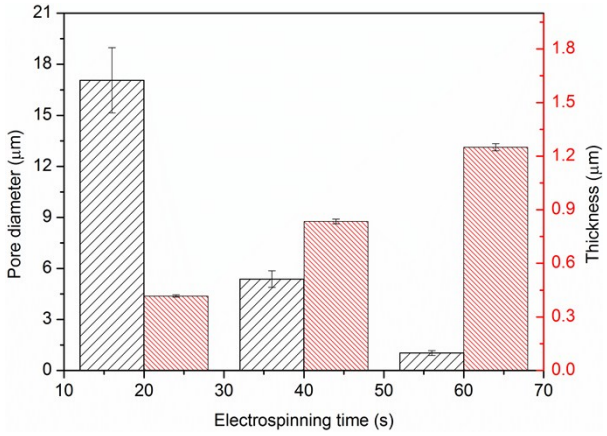

Fig. S2 The pore diameter and thickness of PVDF-HFP membranes for different electrospinning time (20 s, 40 s, 60 s).

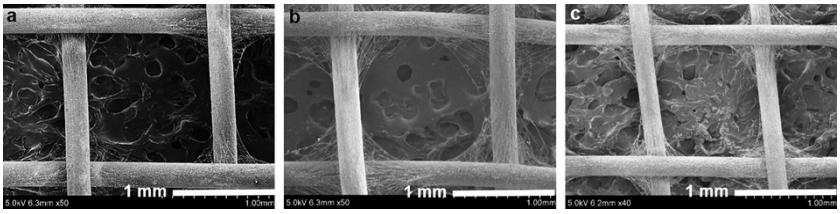

Fig. S3 The hydrophobic surface morphology of the PNJPM-20 (a), PNJPM-40 (b), and JPM-60 (c).

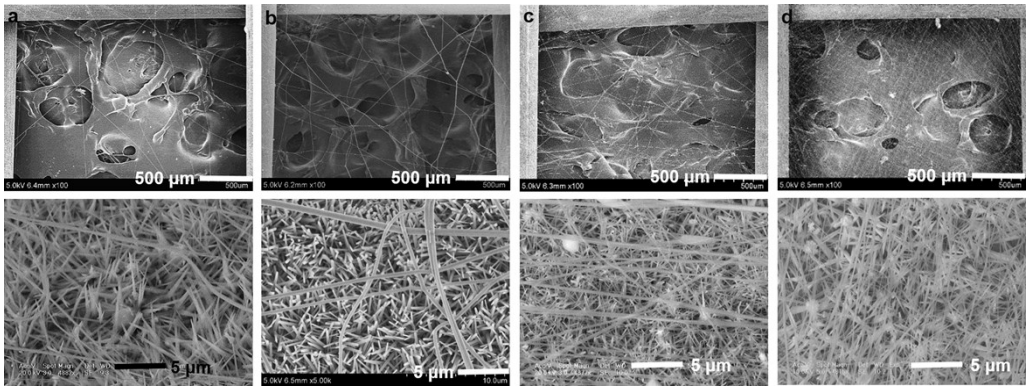

Fig. S4 The hydrophobic surface morphology of the PNJPM-10N (a, electrospinning time of 10 s, no nitrogen blowing), JPM-20N (b, electrospinning time of 20 s, no nitrogen blowing), JPM-40N (c, electrospinning time of 40 s, no nitrogen blowing), JPM-60N (d, electrospinning time of 60 s, no nitrogen blowing).

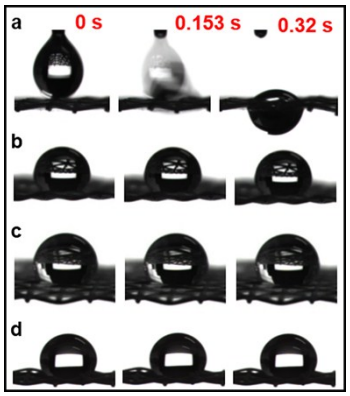

Fig. S5 The unidirectional water (10 μL) transport of PNJPM-10N (a, electrospinning time of 10 s, no nitrogen blowing), JPM-20N (b, electrospinning time of 20 s, no nitrogen blowing), JPM-40N (c, electrospinning time of 40 s, no nitrogen blowing), JPM-60N (d, electrospinning time of 60 s, no nitrogen blowing).

After the N_2 blowing, the nanowire membrane was destroyed by the high pressure, inducing all the PNJPMs possessing the same pore size with the copper mesh (Fig. S3). Before N_2 blowing, the hydrophobic membrane was integrity, covering the copper mesh, causing the pore blocked by the nanowire membrane (Fig. S4). In the absence of nitrogen blowing, the nano-needles pierced the hydrophobic membrane under short electrospinning time (less than 20 s, Fig. S4a). However, they were fully covered by the hydrophobic membrane with longer electrospinning time (greater or equal to 20 s, Fig. S4b-d).

In the absence of the nitrogen blowing, because of the pierced conical nano-needles, the unidirectional water transport of the PNJPM-10N was rapid regardless of the pore size. But they did not unidirectional transport the water for the JPM-20N (electrospinning time of 20 s, no nitrogen blowing, Fig. S5b), JPM-40N (electrospinning time of 40 s, no nitrogen blowing, Fig. S5c), and JPM-60N (electrospinning time of 60 s, no nitrogen blowing, Fig. S5d) without the

piercing conical nano-needles.

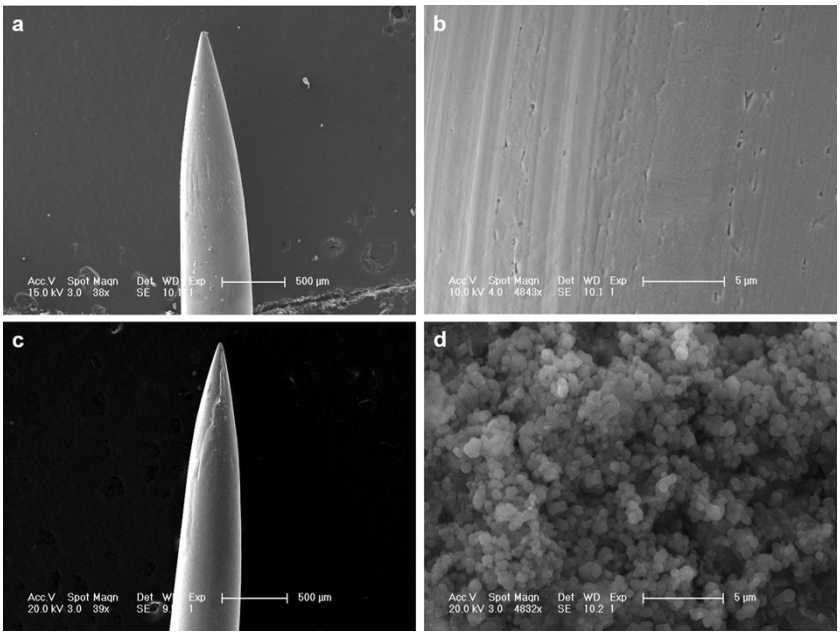

Fig. S6 The morphology of original steel needle (a, b), and hydrophilic steel needle (c, d).

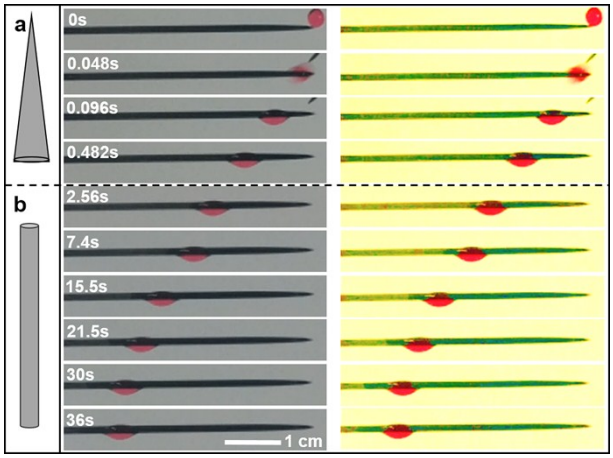

Fig. S7 Water (5 µL, dyed by Reactive Red 120) motions on the hydrophilic steel needle's surface: the water motions at the conical part very rapidly as a result of the structure-Laplace pressure (a), and the water moves at the cylindrical part because of the capillary force (b, little water wetted the surface firstly driving the water movement, the water wetted part is dark green in comparison with the non-wetted part (light yellow)).

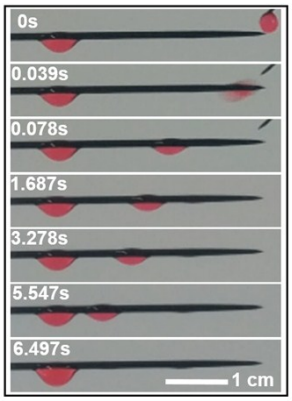

Fig. S8 Due to the lubricant effect, the water (5 μL, dyed by Reactive Red 120) motions on the wetted hydrophilic needle rapidly.

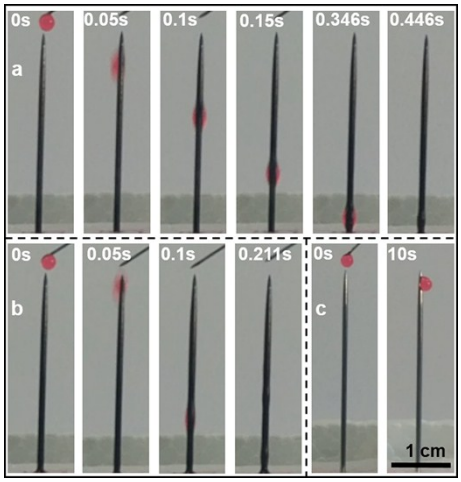

Fig. S9 The dry (a) and wetted (b) hydrophilic vertical placed needle with the gravity transports the water (5 μL, dyed by Reactive Red 120) from tip to base rapidly. The water (5 μL, dyed by Reactive Red 120) hangs on the hydrophobic needle's tip (c).

The steel needle contains two part: the conical part and the cylindrical part. The water could also transport on the cylindrical part. The capillary pressure (P_{cl}) of water on a cylindrical needle (radius, r) can be calculated as: $P_{cl} = -2\gamma \cos\theta / r$ (where θ is the water contact angle (WCA) on cylindrical needle, r is the radius of the cylindrical needle, and γ is the surface tension of water). If the surface is hydrophilic (wettable, WCA < 90°), positive capillary pressure draws the liquid movement along with the cylindrical needle. Induced by the capillary force, the water moves forward on hydrophilic cylindrical part, but the transportation is slower than conical part (Fig. S7). Because of the lubricant effect, the wetted hydrophilic needle (conical part and cylindrical part) enables rapid water movement (Fig. S8). Cooperating with the gravity, the water should motion from the tip to the base much more quickly for the vertical placed needle than horizontal placed needle (Fig. S9a). While the water suspends on the tip for the hydrophobic needle (Fig. S9c). As to the wetted hydrophilic vertical placed needle, the water moves most quickly in all the needles (Fig. S9b).

Fig. S10 The unidirectional water (10 μL) transport of heat oxidized Janus copper mesh (electrospinning time of 10 s, without the pierced nano-needles, no nitrogen blowing).

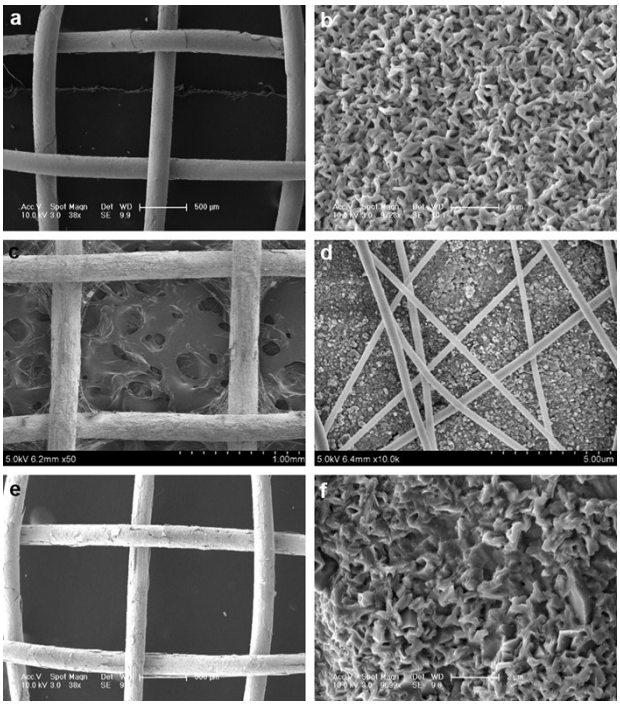

Fig. S11 The morphology of heat oxidized copper mesh (a, b); the hydrophobic surface (c, d) and the hydrophilic surface of the JPM (e, f, electrospinning time of 20 s, nitrogen blowing).

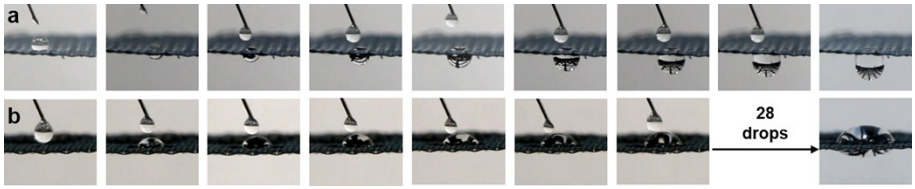

Fig. S12 (a) The water could be unidirectional transported from the hydrophobic surface to the hydrophilic surface continuously (PNJPM-20, 10 μL drop^{-1}); (b) the water could be blocked on hydrophilic surface continuously (PNJPM-20, 10 μL drop^{-1}).

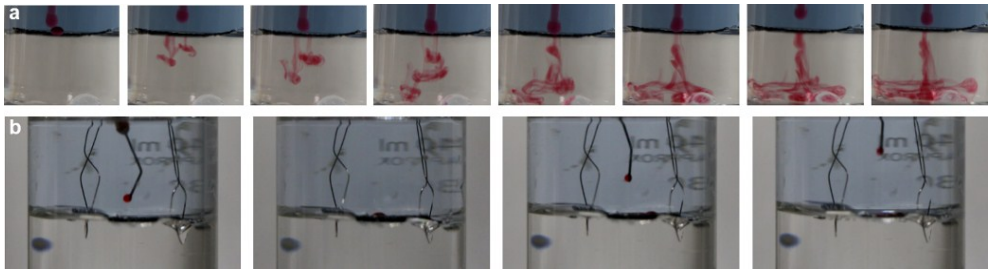

Fig. S13 (a) The CCl_4 drops (10 μL/drop, dyed by oil red) are directional transported from the hydrophilic surface to the hydrophobic surface at the water (dyed by methylene blue)-oil (CCl_4) interface continuously (PNJPM-20); (b) The CCl_4 drops (10 μL/drop, dyed by oil red) are blocked from the hydrophobic surface to the hydrophilic surface at the water (dyed by methylene blue)-oil (CCl_4) interface continuously where the PNJPM-20 is fixed at the water-oil interface by a wire.

The solution oxidized copper mesh (hydrophilic) is underwater-superoleophobic[1], and the hydrophobic PVDF-HFP is oleophilic, triggering the PNJPM-20 act as the oil-diode in liquid-liquid system. Bioinspired by the Janus lotus leaf floating on the water-oil interface naturally[2], the PNJPM-20 also floats spontaneously with the hydrophilic surface upward at the water-oil (CCl_4) interface (Fig. S13a). In addition, the oil drops (CCl_4, 10 μL drop^{-1}) could penetrate from the

superoleophobic surface (hydrophilic) to the oleophilic surface (hydrophobic) continuously (Fig. S13a). However, the PNJPM-20 could sink in the oil (CCl_4) with the hydrophobic surface upward, the oil suspends on the hydrophobic surface without penetration (Fig. S13b). When the hydrophobic surface is upward, there may be a layer of air between the water and hydrophobic surface forming the water-air-solid tri-phase, and the oil threads through the air phase and suspends on the copper mesh.

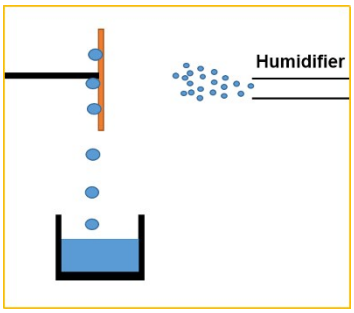

Fig. S14 Schematic illustration of the homemade water-collecting system.

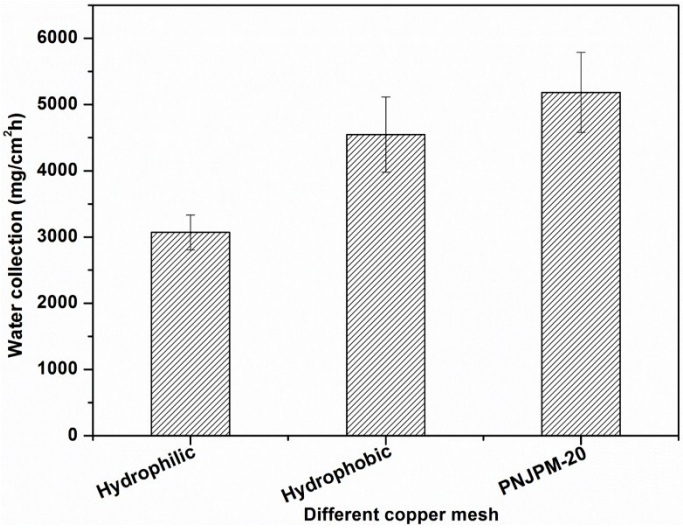

Fig. S15 Water collection efficiency of three different membranes (Hydrophilic copper mesh (mesh number: 16): solution oxidized; Hydrophobic copper mesh (mesh number: 16): solution oxidized, and then cured at dodecyl mercaptan solution for 6 h).

As a result of the rapid unidirectional water transport, the PNJPM maybe possess the enhanced fog collection ability. To test the fog collection ability, the membranes were vertically fixed in a fog flow (Fig. S14). After 5 min of fogging, the collected water was weighed and analyzed. Enhanced fog collection ability was observed on the PNJPM-20. In the same time interval, the water collection rate by the Janus system was 1.8 and 1.3 times more than that of the hydrophilic and hydrophobic mesh, respectively (Fig. S15).

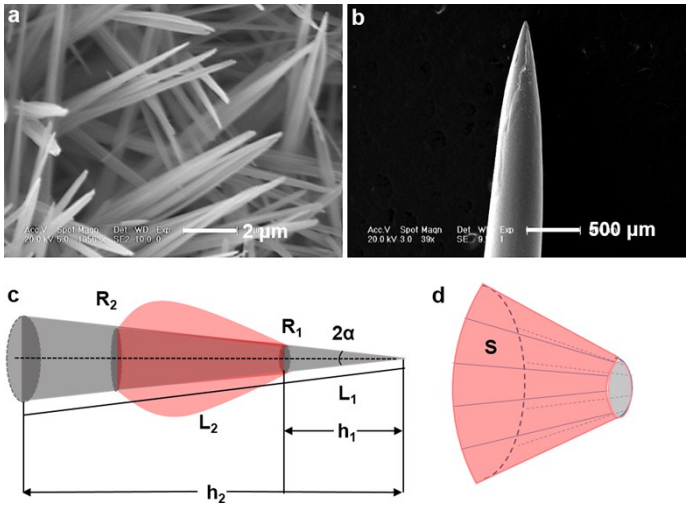

Fig. S16 The conical nanometer-sized (a) and centimeter-sized needle (b). (c) Mechanism of water drop motion on hydrophilic conical needle. (d) The water wetted area of hydrophilic needle (S is barrel shape of hydrophilic needle).

The structure-Laplace pressure of hydrophilic conical needles can be described in the following equation:

$$F_{hydrophilic-Laplace} \approx \gamma \cdot (1/R_1 - 1/R_2) \cdot S \approx \frac{\gamma \cdot \pi \cdot (R_2 L_2 - R_1 L_1) \cdot (R_2 - R_1)}{R_1 R_2}$$

Where γ is the surface tension of water, R_1 and R_2 are the local radii of the needle at the opposite sides of the water drop (Fig. 16c). Element of cone is L_1 and L_2 (Fig. 16c). h_1 and h_2 are the height (Fig. 16c). S represents the water infused area, namely the barrel-shaped area, for the hydrophilic conical needle (Fig. 16d).

Assuming R_1 is much less than R_2.

$$F_{\text{hydrophilic}-Laplace} \approx \frac{\gamma \cdot \pi \cdot h_2^{\,2} \cdot Sin(\alpha)}{R_1 Cos^2(\alpha)}$$

Assuming R_1 is infinitely small, where the R_1 is same with each other for different conical needles (centimetre-sized and nano-sized conical needles).

$$\frac{F_{centimeter}}{F_{nanometer}} = \frac{h_c^{\,2} \cdot Sin(\alpha_c) \cdot Cos^2(\alpha_n)}{h_n^{\,2} \cdot Sin(\alpha_n) \cdot Cos^2(\alpha_c)}$$

Where $F_{centimeter}$ and $F_{nanometer}$ are the centimetre-sized and nanometer-sized conical needles' structure-Laplace pressure, respectively.

As to the nanometer-sized needle: h_n=6.4 μm and α_n=0.0011° (Fig. S16a), while the centimeter-sized needle: h_c=2 mm and α_c=0.675° (Fig. S16b). Then, the driving force for the centimeter-sized needle is $6*10^7$ time more than the nanometer-sized needle's. From SEM images, there is thousands of nanometer-needles on the surface of the PNJPM, forming the large structure-Laplace pressure inducing the rapid unidirectional water transport.

Table S1 Different Janus membranes with different unidirectional water transportation rate

Janus membrane	Drops (μL)	Time (s)	Rate (μL/s)	Reference

Cotton fabric	10	0.96	10.42	3
Copper mesh	12	0.87	13.8	4
Cotton fabric	20	9.62	2.08	5
Polyester fabric	40	2.25	17.78	6
Cotton fabric	40	1.4	28.57	7
Cotton fabric	60	4.2	14	8
Electrospinning membrane	100	3.5	28.57	9
PNJPM-20	10	0.31	32.26	This work
PNJPM-20	20	0.37	54.05	This work
PNJPM-20	40	0.34	117.65	This work
PNJPM-20	60	0.29	206.9	This work
PNJPM-20	80	0.28	285.7	This work
PNJPM-20	100	0.34	294.12	This work

References

1. F. Zhang, W. B. Zhang, Z. Shi, D. Wang, J. Jin and L. Jiang, *Adv. Mater.*, 2013, 25, 4192-419.
2. Y. Y. Zhao, C. M. Yu, H. Lan, M. Y. Cao and L. Jiang, *Adv. Funct. Mater.*, 2017, 27, 1701466.
3. H. Zhou, H. Wang, H. Niu and T. Lin, *Sci. Rep.*, 2013, **3**, 1-6.
4. H. Li, M. Y. Cao, X. Y. Ma, Y. X. Zhang, X. Jin, K. S. Liu and L. Jiang, *Adv. Mater. Interfaces*, 2016, **3**, 1600276.
5. X. L. Tian, H. Jin, J. Sainio, R. H. A. Ras and O. Ikkala, *Adv. Funct. Mater.*, 2014, **24**, 6023-6028.
6. C. Zeng, H. X. Wang, H. Zhou and T. Lin, *Adv. Mater. Interfaces*, 2016, **3**, 1600036.
7. H. X. Wang, J. Ding, L. M. Dai, X. G. Wang and T. Lin, *J. Mater. Chem.*, 2010, **20**, 7938-7940.
8. H. Zhou, H. X. Wang, H. T. Niu, C. Zeng, Y. Zhao, Z. G. Xu, S. D. Fu and T. Lin, *Adv. Mater. Interfaces*, 2016, **3**, 1600283.
9. J. Wu, N. Wang, L. Wang, H. Dong, Y. Zhao and L. Jiang, *Soft Matter*, 2012, **8**, 5996-5999.